

(Preprint) AAS 18-244

< = ; < ' : = 8 9 @ @ H M = U B ' D F C G 5 G G = A 5 9 B ;
6 F I H 9 ' : C F 7 9 ' A C B G 9 G 7 A I @ 5 H = C B G

**Doyle T. Hall*, Stephen J. Casali*, Lauren C. Johnson*, Brent B. Skrehart*
and Luis G. Baars***

The NASA Conjunction Assessment Risk Analysis team has implemented new software to estimate the probability of collision (P_c) for Earth-orbiting satellites. H \ Y ' U ' [c f] h \ a ' Y a d ' c m g ' U ' I V f i h Y ' Z c f W Y ' A c b h Y ' 7 U f ' offers from most other methods because it uses orbital states and covariances propagated from their orbit determination epoch times using the full set of the Astrodynamics Support Workstation's higher order theory models, including the High Accuracy Satellite Drag Model. This paper describes the BFMC algorithm, presents comparisons of BFMC P_c estimates to those calculated using other methods, and discusses the implications for conjunction risk assessment.

INTRODUCTION

The NASA Conjunction Assessment Risk Analysis (CARA) team estimates probabilities of collision for a specific set of high value Earth-orbiting satellites. The CARA processing system first detects candidate close encounters up to ten days in advance using a screening-volume approach based on the latest available satellite tracking data and orbit determination (OD) state and covariance solutions.^{1,2} For each candidate conjunction, CARA assesses the collision risk using a set of well-established semi-analytical P_c estimation methods^{3,4} which are relatively computationally efficient because they employ several simplifying assumptions, including linear trajectories. Unfortunately, such methods can potentially fail to provide accurate P_c estimates for specific conjunction geometries, including long-term or repeating encounters between closely spaced objects.⁴ These specific conjunctions can be addressed using Monte Carlo (MC) simulations.⁵

The CARA team has implemented software to calculate P_c Y g h] a U h Y g ' Y a d ' c m] b [' U ' I A c b h Y ' of BFMC algorithm. The method can be computationally intensive because it uses high fidelity Special Perturbations (SP) orbital propagation⁶ within an MC approach that has been described in detail previously.⁷ Specifically, the most advanced mode of the BFMC software repeatedly performs the following algorithmic steps: 1) sample SP states from their probability density functions (PDFs) of the primary and secondary satellites at their respective OD epoch times; 2) use these sampled SP states to propagate high fidelity estimates of the state vectors of two satellites forward in time throughout the entire period of interest for collision risk assessment, explicitly checking if the intervening distance ever becomes less than the combined 'hard-body' radii of the two satellites; and 3) if so, register that a simulated collision has occurred at the time of first contact between the two spheres defined by those radii. These steps need to be repeated until sufficient simulated collisions have been registered to provide a P_c estimate to a desired accuracy.

* Research Analyst, Omitron Inc., 555 E. Pikes Peak Ave, #205 Colorado Springs, CO 80903.

The BFMC algorithm differs from most other P_c estimation methods in two ways. First, it uses complete SP orbital states and covariances, enabling high fidelity trajectory propagation. Second, in its most advanced mode of operation, BFMC uses only the SP states and covariances estimated at the OD epoch times, instead of relying on states and covariances predicted at the nominal time of closest approach (TCA) for the conjunction. The SP states comprise six equinoctial orbital elements, supplemented by two additional state parameters that account for the effects of orbital perturbations, including atmospheric drag and solar radiation pressure.^{6,7}

Because BFMC employs SP states and equinoctial orbital elements natively, it can be used for studying P_c inaccuracies introduced by using Cartesian or other state representations.⁷ BFMC also incorporates the latest version of the Jacchia-Bowman atmospheric density model⁸ plus the associated Dynamic Calibration Atmosphere (DCA) for the High Accuracy Satellite Drag Model (HASDM)⁹ and exactly matches the currently operational SP software configuration of the Astrodynamics Support Workstation (ASW).^{10,11} Great care has been taken to ensure that all SP propagations are performed using the most recent and accurate input data, including the latest updates available for orbital states and atmospheric parameters.

This paper describes the BFMC algorithm in detail, presents comparisons of the high fidelity BFMC P_c estimates to those calculated using other methods, and discusses the implications for satellite conjunction risk assessment.

PREVIOUS WORK

Collision probabilities between tracked Earth-orbiting satellites have been discussed extensively during the past few decades, including methods that use semi-analytical approaches as well as more computationally intensive Monte Carlo approaches.

Semi-Analytical Collision Probability Methods

Many authors have formulated and discussed semi-analytical P_c methods (see references 3, 4, 12-18, and references therein). In 1992, Foster and Estes³ introduced a method that employs three simplifying assumptions: 1) the relative satellite motion can be approximated as linear during the conjunction, 2) the uncertainties on the relative satellite positions during the conjunction can be approximated using a single, constant covariance matrix, and 3) the uncertainties on the satellite velocities can be neglected altogether. These assumptions make the mathematical problem significantly more tractable, and ultimately allow P_c values to be approximated semi-analytically using 2-dimensional (2D) numerical integration.^{3,4} In 2000, Akella and Alfriend⁹ also employed these assumptions and reformulated the theory to demonstrate that the collision probability can be alternatively be expressed as an integral over time

(1)

where the integrand represents a collision probability rate (also see reference 15), which can itself be calculated using 2D numerical integration. In a linear-motion encounter, only one close approach (CA) occurs, meaning that has a single peak in time, so the integration limits can be taken as and . Akella and Alfriend¹² show that the infinitely-bounded time integral part of the expression above can be performed analytically, ultimately yielding an expression for P_c with the same form as originally presented by Foster and Estes.³

Most conjunctions between tracked satellites can be approximated accurately using methods of Foster and Estes³ and Akella and Alfriend.¹² However, some conjunctions do not sat-

isfy all three of the 2D P_c assumptions stated above, and must be addressed using a different approach.^{4,5} Several authors have formulated semi-analytical approaches relaxing the 2D P_c assumptions.^{4,13-18} This analysis focuses on using MC methods for this purpose.

Monte Carlo Collision Probability Methods

Collision probabilities can be estimated using MC simulations.^{5,7} These can be computationally intensive because they require repeatedly performing the following steps: 1) sample the orbital state PDFs of the primary and secondary satellites; 2) use the sampled states to propagate state vectors throughout the risk assessment period, determining if the distance between the objects ever becomes less than a combined hard-body protection radius; and 3) if so, register that a simulated collision has occurred.¹⁹ These steps need to be repeated until enough collisions have been registered to provide sufficiently accurate statistical results, which may require a large number of samples depending on the conjunction. Step 2 requires the most computation, especially for propagation schemes that use complex dynamical models.

In 2011, Sabol *et al.*⁷ described an MC approach using high fidelity SP orbital propagation, which employs a complex and accurate special perturbations dynamical model.^{6,10,11} That analysis describes two important aspects of the SP MC approach. First, using a Cartesian orbital state representation in the simulations should be avoided because it inaccurately models satellite state uncertainties – a drawback not suffered when using an SP state representation expressed in equinoctial orbital elements supplemented by additional state parameters.^{7,20-22} Second, SP state sampling and propagation can be performed in two distinctly different ways.⁷ States can be sampled from PDFs estimated at the OD epoch times for the primary and secondary satellites, and then propagated forward in time throughout a collision risk assessment period. Alternatively, states can be sampled from PDFs predicted for a WC b ^ i b Wh] TCA and propagated forward and backward from that point in time. In this analysis, these two sampling/propagation approaches will be referred to U g ^ f Y d f Y g Y b h g ^ 6 : P_c Z b n g i a n o d e , h a n d U g g c \

BRUTE FORCE MONTE CARLO COLLISION PROBABILITY ALGORITHM

The BFMC algorithm presented here extends the method originally developed by Sabol *et al.*⁷ so that it can be applied to actual conjunctions experienced by 7 5 F 5 s e t o f protected primary satellites. The BFMC software has two fundamental modes of operation, corresponding to the from-epoch and from-TCA sampling/propagation approaches discussed above. The from-epoch approach ^ f Y d f Y g Y b h g ^ 6 : P_c Z b n g i a n o d e , h a n d U g g c \

Special Perturbations Orbital States and Covariances

An SP orbital state is represented by an 8^1 column vector, , with the first six elements denoting h \ Y ^ g U e q u i n o c t i a l o r b i t a l e l e m e n t s , and the last two a ballistic coefficient plus a solar radiation pressure parameter.^{6,23-25} The ASW OD process^{2,6,10,11} analyzes multiple tracking observations of a satellite to estimate a mean state, , at an OD epoch time, . (This analysis uses a g i V g W f] d h ^ f \$ I ^ h c ^ X Y b c h Y ^ e i U n o n l y w h e n required for clarity.) The epoch typically coincides with the time of the latest tracking observation incorporated into the OD analysis.

The actual state for a satellite at epoch differs from the estimated mean state because of measurement and modeling uncertainties, , and the OD process also provides an estimate of the 8^8 covariance matrix, .^{2,6,10,24,25} The epoch state uncertainty PDF can be

approximated $\mathbf{g} \sim \mathbf{b} \mid \mathbf{U}; \mathbf{U} \mid \mathbf{g} \sim \mathbf{f}^2 \mathbf{Y} \mathbf{d} \mathbf{f} \mathbf{Y} \mathbf{g} \mathbf{Y} \mathbf{b} \mathbf{h} \mathbf{U} \mathbf{h} \mid \mathbf{c} \mathbf{b} \mathbf{z}$, where \mathbf{g} denotes a multi-variate normal (MVN) function

$$\mathbf{Y} \mid \mathbf{g} \sim \mathbf{f}^2 \mathbf{Y} \mathbf{d} \mathbf{f} \mathbf{Y} \mathbf{g} \mathbf{Y} \mathbf{b} \mathbf{h} \mathbf{U} \mathbf{h} \mid \mathbf{c} \mathbf{b} \mathbf{z} \quad (2)$$

The epochs, mean states and covariances can be derived from the *Vector Covariance Message* (VCM) produced by the ASW OD processing system.^{10,11}

The SP epochs, mean states and covariances for the primary and secondary objects involved in a conjunction are denoted here as \mathbf{g}_p and \mathbf{g}_s , respectively. (This analysis is $\mathbf{g}_p \mathbf{Y} \mathbf{g}_s \mid \mathbf{V} \mathbf{g} \mathbf{W} \mathbf{f} \mid \mathbf{d} \mathbf{h} \mathbf{g} \mid \mathbf{f} \mathbf{g} \mathbf{U} \mathbf{b} \mathbf{X} \mid \mathbf{f} \mathbf{g} \mathbf{U} \mathbf{b} \mathbf{h} \mid \mathbf{h} \mathbf{Y}$ again, only when required for clarity.) Typically, the two OD epochs do not coincide, and both typically precede the nominal conjunction TCA by 0.5 to 10 days in CARA processing. Because VCMs for both the primary and secondary object are used as inputs for from-epoch pro- $\mathbf{W} \mathbf{Y} \mathbf{g} \mathbf{g} \mid \mathbf{b} \mathbf{z} \mid \mathbf{d} \mathbf{A} \mathbf{c} \mathbf{W} \mathbf{d} \mathbf{g} \mathbf{a} \mathbf{Z} \mathbf{c} \mathbf{f} \mathbf{X} \mathbf{c} \mathbf{Y} \mathbf{a} \mid \mathbf{g} \mathbf{U} \mathbf{g} \mathbf{c} \mathbf{f} \mathbf{Y} \mathbf{Z} \mathbf{Y} \mathbf{f} \mathbf{f} \mathbf{Y} \mathbf{X} \mathbf{h} \mathbf{c} \mathbf{U} \mathbf{g} \mathbf{f} \mathbf{J} \mathbf{7} \mathbf{A}$

Special Perturbations Propagation

SP states can be propagated to predict high fidelity future Earth-Centered Inertial (ECI) reference frame satellite position vectors,⁶ denoted symbolically here as \mathbf{g} , where \mathbf{g} represents an ensemble of model and environmental data sets required for SP propagation. (The contents of \mathbf{g} are described in more detail later.) Similarly, SP mean states and covariances can be propagated^{6,23-25} and denoted symbolically as \mathbf{g}_p and \mathbf{g}_s , respectively. Note, in this analysis some or all of the function arguments listed to the right of semicolons may be suppressed for brevity. For example, a position vector might be expressed in one of the following three ways:

Sampled Orbital States

Samples can be drawn from an MVN PDF by applying Eigen-decomposition to the covariance matrix²⁶

(3)

where \mathbf{U} is a unitary matrix containing orthogonal eigenvector columns, $\mathbf{\Lambda}$ is a diagonal matrix of associated eigenvalues, \mathbf{z} . The k^{th} sampled state, \mathbf{g}_k , can be generated using

(4)

where \mathbf{z} represents a set of independent normal deviates²⁷ (such as those returned by MATLAB `randn` function). This sampling method fails for non-positive definite (NPD) covariances, for which $\mathbf{\Lambda} \not\geq \mathbf{0}$, because it produces states with non-zero imaginary components. Previous analysis indicates²⁶ that such NPD covariances have a variety of causes, and typically possess just one negative eigenvalue that is only slightly negative relative to the largest eigenvalue. NPD SP state epoch covariances, \mathbf{C} , occur very rarely in CARA processing; NPD propagated covariances, \mathbf{C}_p , occur somewhat more often, especially for long propagation intervals. BPMC avoids NPD-induced sampling failures by replacing \mathbf{C} in eq. (4) with $\mathbf{C} \mathbf{S}$.²⁶

Simulated Collisions

6 : A 7 from-epoch, VCM mode simulates collisions by using sampled primary and secondary SP states to propagate state vectors forward in time from their OD epochs, explicitly checking if the intervening distance between the two objects ever becomes less than a threshold miss distance, d_{thr} . (Ideally, d_{thr} represents the combined hard-body radii of the two objects, if both are known, but

also can represent an imposed hard-body protection distance) BFMC repeats this process for a large number of sampling trials, N . For each trial, BFMC generates independently sampled SP states for the primary and secondary objects, \mathbf{r}_p and \mathbf{r}_s , respectively. The current BFMC implementation does not reuse any state samples or propagations during the simulation; such reuse can increase the efficiency of MC calculations significantly, but also can lead to underestimated confidence intervals.²⁸

The time-dependent intervening distance between the two objects for the k^{th} trial can be written

(5)

For a risk assessment interval $[t_0, t_1]$, the CA distance and time for the k^{th} trial can be found numerically as follows:

$$\mathbf{r}_p(t) = \mathbf{r}_p(t_0) + \mathbf{v}_p(t - t_0) \quad \mathbf{r}_s(t) = \mathbf{r}_s(t_0) + \mathbf{v}_s(t - t_0) \quad (6)$$

If $\mathbf{r}_p(t) \cdot \mathbf{r}_s(t) > 0$, then no collision could have occurred during the interval. However, if $\mathbf{r}_p(t) \cdot \mathbf{r}_s(t) < 0$, then a collision must have occurred. In general, BFMC registers a simulated collision for the k^{th} trial if and only if there exists a [time of first contact] t_c which is carefully defined here as the earliest time that simultaneously satisfies the following three conditions:

$$\mathbf{r}_p(t_c) \cdot \mathbf{r}_s(t_c) = 0 \quad \mathbf{v}_p(t_c) \cdot \mathbf{r}_s(t_c) < 0 \quad \mathbf{v}_s(t_c) \cdot \mathbf{r}_p(t_c) < 0 \quad (7)$$

The first condition requires the two hard-body spheres to be in contact, the second that the objects be approaching one another, and the third that the contact occurs during the specified risk assessment interval. Trials that X c b c h d c g g Y g g g i W \ U Z] f g h W c b h U W h h collision occurs during the risk assessment interval. Each trial that does have a first contact time constitutes a simulated collision or [\] which is registered as occurring at the time of first contact. The computed number of hits for all trials can be denoted N_{hits} , or just N for brevity.

BFMC From-Epoch or VCM Mode Collision Probabilities

Dividing the number of hits by the number of sampling trials yields the best-estimate collision probability from the MC simulation

(8)

If $N_{\text{hits}} = 0$ and $N = 0$, then the 95% confidence interval on this estimate can be approximated as $[0, 0]$, but a more accurate, asymmetric confidence interval can be estimated for all $N_{\text{hits}} > 0$ using the Clopper-Pearson method^{29,30} (e.g., MATLABD `binofit` function) or other methods.³¹

Because of the careful definition of the first contact time, t_c , this collision probability algorithm can be applied to arbitrarily short or long time intervals, $[t_0, t_1]$, and will always yield a number of hits in the range $0 \leq N_{\text{hits}} \leq N$, and a best-estimate probability in the range $0 \leq P \leq 1$. For temporally-isolated conjunctions, BFMC should be applied to a time interval that closely brackets the single peak in probability rate, but remains sufficiently wide to obtain an accurate total probability estimate.^{19,32} However, for closely-spaced orbiting objects, which can have long-duration and/or repeating conjunctions,^{18,19,33} the interval can be extended to span an arbitrarily large number of probability rate peaks" $H \setminus] g a Y U b g h \setminus U h 6 : A 7 \textcircled{D} g J 7 \text{self-} a c X Y \setminus] g$ consistent, multi-day risk assessments even for this difficult class of satellite interaction. The CARA team continues to analyze how to use BFMC optimally to estimate probabilities for such extended, multi-encounter interactions. This analysis, however, restricts application of BFMC to

temporally-isolated conjunctions for which a time interval Δt can be defined that closely brackets a single peak in probability rate (as shown in the bottom panels of Figures 1 and 4).

BFMC From-Epoch or VCM Mode Collision Probability Rates

Because the algorithm presented above can be used for time intervals of arbitrary duration, it can also be applied to a sequence of very short time intervals, or bins, that jointly span the entire risk assessment period. This allows MC collision probability rates to be estimated as follows. Equally spaced time bin mid-points can be defined as t_j , where $j = 1, 2, \dots, N_s$ and N_s is the number of bins. The computed number of hits within the j^{th} bin can be denoted as N_j , allowing the collision rate at any time during the risk assessment interval to be estimated by averaging over each bin:

$$\hat{P}_c = \frac{1}{N_s} \sum_{j=1}^{N_s} N_j \Delta t \quad (9)$$

It is straightforward to show that integrating \hat{P}_c from t_1 to t_2 yields

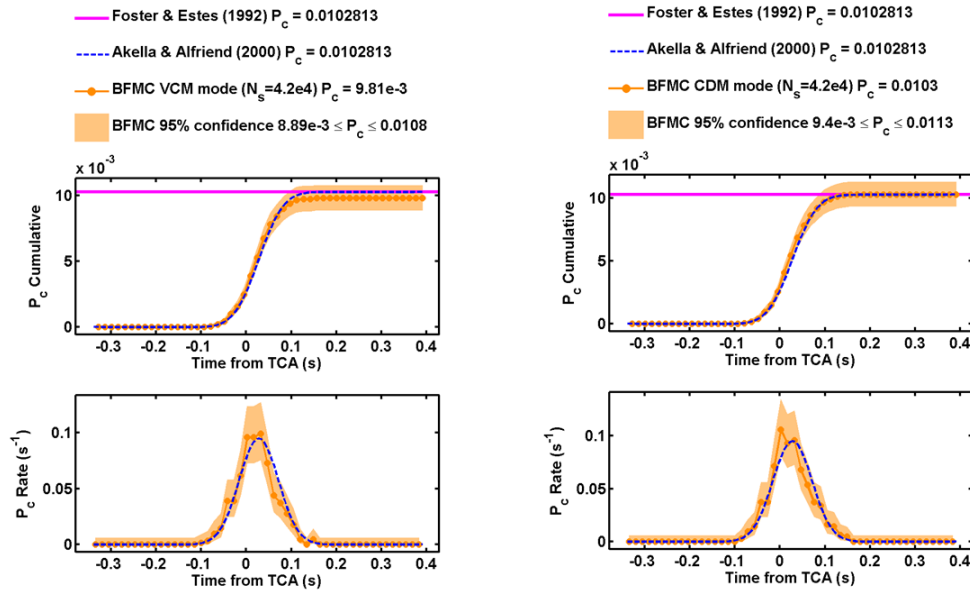


Figure 1. Estimated cumulative P_c (top panels) and P_c rate (bottom panels) for VCM mode (left panels) and CDM mode (right panels), for a Wc b ^ i b Wh] c b ^ V Y h k Y Y b ^ B 5 G 5 D g ^ 5 e i U ^ g Aqua satellite and a debris object.

Figure 1 shows plots of BFMC collision probabilities and probability rates estimated using equations (8) and (9), respectively, for a Wc b ^ i b Wh] c b ^ V Y h k Y Y b ^ B 5 G 5 D g ^ 5 e i U ^ g debris object. Specifically, the top left panel shows VCM mode P_c estimates, and the bottom left panel shows VCM mode P_c rate estimates. Orange dots show estimates for each bin and the light orange shaded region represents associated 95% confidence uncertainty intervals.²⁹ Figure 1 also shows 2D P_c estimates^{3,12} which agree well with the BFMC estimates, as is the case with the vast majority of the temporally-isolated conjunctions analyzed here (discussed in more detail later).

BFMC From-TCA or CDM Mode Collision Probabilities and Rates

The discussion above focuses on the from-epoch sampling/propagation approach using VCM mode. This approach uses a from-TCA approach that is significantly less computationally intensive. Because all input data required for from-TCA processing can be derived from a *Conjunction Data Message* (CDM),^{19,26,33} this is also called

6 : A 7 D g J 7 A a 8 X SP state vectors from estimated OD-epoch PDFs and uses those states to calculate position vectors with high-fidelity SP propagation. 6 : A 7 CDM mode differs in two fundamental ways. First, it samples $6^{\wedge}1$ equinoctial element state vectors from marginalized PDFs predicted at the WC b ^ i b nominal TCA. Second, it propagates orbital states using computationally efficient Keplerian 2-body equations of motion. As explained earlier, an SP mean state predicted at TCA is denoted $(\hat{\mathbf{x}}_T)$. The first six elements of this $8^{\wedge}1$ vector represent the best-estimate prediction for the mean equinoctial state, denoted here as the $6^{\wedge}1$ vector $\hat{\mathbf{x}}_T$. (In this analysis, primes denote TCA, equinoctial state quantities). Similarly, the $8^{\wedge}8$ SP covariance matrix predicted at TCA is denoted $(\hat{\mathbf{P}}_T)$. The upper-left $6^{\wedge}6$ part of this matrix represents the marginalized equinoctial state covariance, denoted here as $\hat{\mathbf{P}}_T$.

TCA equinoctial element states and covariances for the primary and secondary objects, $(\hat{\mathbf{x}}_T)$ and $(\hat{\mathbf{P}}_T)$, respectively, can be derived from a CDM. Predicted position vectors propagated from these TCA equinoctial states using 2-body equations of motion^{6,23,24} are denoted here as $\hat{\mathbf{r}}_T$ and $\hat{\mathbf{r}}_T$. In the same way as described in the previous sections, but with these CDM mode quantities substituted for their original VCM mode counterparts. Specifically, the nominal TCA for the conjunction should be substituted for both epoch times t_1 and t_2 ; the position vector $\hat{\mathbf{r}}_T$ should be substituted for $\hat{\mathbf{r}}_1$; for $\hat{\mathbf{r}}_2$; for $\hat{\mathbf{r}}_3$; etc.

Because the CDM mode employs 2-body propagation, it must be restricted to relatively short risk assessment intervals $b Y U f ^ h \setminus Y ^ W c b ^ i b$, which is the objects orbital perturbations that can affect the orbital motion over longer time scales. For this reason, CDM mode can only be applied to temporally-isolated conjunctions with durations^{4,32} that are very short relative to the minimum orbital period of the two objects.¹⁹ This restriction does not apply to 6 : A 7 D g VCM mode, because it employs only high fidelity SP propagation. CDM mode risk assessment time intervals could conceivably be extended if a higher-fidelity propagator were used, as would be required for extended or repeating events. However, any situations in which the CDM mode 2-body approach would be inadequate can already be addressed by 6 : A 7 VCM mode.

The right panels of Figure 1 show \hat{P}_c and \hat{P}_c estimates produced by 6 : A 7 CDM mode. Figure 1 demonstrates that the VCM and CDM modes produce statistically equivalent results for this conjunction. This CDM vs VCM mode equivalence has been found to hold for all temporally-isolated conjunctions analyzed so far, as discussed in detail later. Figure 1 also demonstrates that, for this Aqua satellite conjunction, both BFMC estimates agree well with the 2D P_c approximation: $VCM-P_c \approx CDM-P_c \approx 2D-P_c \approx 10^{-2}$. This BFMC vs 2D P_c equivalence has been found to hold for the vast majority of temporally-isolated conjunctions analyzed here, but a small fraction show statistically significant differences, also discussed in detail later.

BRUTE FORCE MONTE CARLO SOFTWARE IMPLEMENTATION

The main BFMC software module encodes the sampling, propagation, and collision simulation algorithms described above, implemented in compiled FORTRAN that links with ASW software libraries.¹⁰ In addition, a set of pre-processing modules collect and assemble the input data required

Accounting for Cross Correlated Orbital State Estimates

The BFMC algorithm presented above assumes that the OD-epoch state uncertainty PDF covariances for the primary and secondary objects are statistically independent. However, because of the way OD processing is performed,^{2,6} estimated orbital state covariances can be correlated due to the use of common force-model parameters, common tracking system biases, etc.³⁴ Such correlations can affect P_c estimates.^{34,35} The BFMC processing system naturally lends itself to correcting for cross correlation effects caused by common force-model parameters – in particular, those within the global atmospheric density model used for both state estimation and state prediction.⁸ A companion BFMC paper presented at this conference by Casali *et al.*³⁵ formulates a method that uses the atmospheric data collected and assembled within to account for such cross correlations in the state prediction portion of the process. For most conjunctions, accounting for such prediction-phase cross correlation effects has a relatively small effect on P_c estimates. However, for conjunctions involving satellites experiencing appreciable atmospheric drag, P_c values can be increased or decreased significantly.³⁵ The current analysis assumes for simplicity that the covariances have negligible cross correlation, focusing on the comparison of different MC P_c estimation methods rather than eradicating cross correlation effects in the calculation.

Measurements of Computation Speeds

Because CDM mode employs efficient 2-body propagation, it computes more quickly than the VCM mode, which employs high fidelity SP propagation. Performance measurements using a 24 CPU core Linux workstation show that CDM mode can calculate at a rate of about 100 sampling trials per second using a single core. VCM mode single-core computation rates depend inversely on the summed propagation times for the primary and secondary as follows

$$\frac{1}{\text{rate}} = \frac{1}{N} \left(\frac{1}{\text{rate}_1} + \frac{1}{\text{rate}_2} \right) \quad (10)$$

So for an isolated conjunction in which both OD epochs precede the nominal TCA by twelve hours, i.e., $(t_1 - t_0) = (t_2 - t_0) = 12$ hours, about 10 VCM mode trials can be calculated per second using a single core. Using 20 cores in parallel increases this to about 200 trials per second.

Table 1. Approximate BFMC execution times for a workstation using 20 CPU cores, estimating P_c values to an accuracy of about 20% with 95% confidence.

	$P_c = 10^{-4}$	$P_c = 10^{-5}$	$P_c = 10^{-6}$	$P_c = 10^{-7}$
CDM Mode	0.5 seconds	5 seconds	50 seconds	8.3 minutes
VCM (1 PROPday)	1.4 hours	14 hours	5.8 days	58 days
VCM (10 PROPdays)	14 hours	5.8 days	58 days	580 days

Estimating P_c values to an accuracy of about 20% with 95% confidence usually requires 100 hits (which also yields a 1 σ accuracy of about 10%). For a conjunction with $P_c = 10^{-4}$, this requires 100 sampling trials, which can be computed using CDM mode with 20 cores in about 0.5 seconds. For $P_c = 10^{-5}$, 1000 trials are needed, which can be computed in about 5 seconds. For $P_c = 10^{-6}$, 10,000 trials are needed, which can be computed in about 50 seconds. For $P_c = 10^{-7}$, 100,000 trials are needed, which can be computed in about 8.3 minutes. The majority of important CARA conjunctions have total propagation times less than 10 days.

The CDM mode is faster than the VCM mode, depending on the conjunction. This relative CDM/VCM mode speed

A binomial proportion test can be used to test the hypothesis that BFA 7 \cap g \cap 7 8 A \cap a c X mode produce the same P_c estimates, i.e., to test the null hypothesis that two binomial proportions are equal.³⁶ Applying this test to each of the 373 cases plotted in Figure 2 indicates that none violates the null hypothesis with a statistical test p-value $\geq 10^{-3}$. In other words, no points deviate from the 45% dashed line in the upper panel of Figure 2 at this high level of statistical confidence. Additional testing of selected conjunctions using much larger numbers of sampling trials (e.g. Figure 4) also indicates that the CDM and VCM modes produce statistically equivalent P_c estimates.

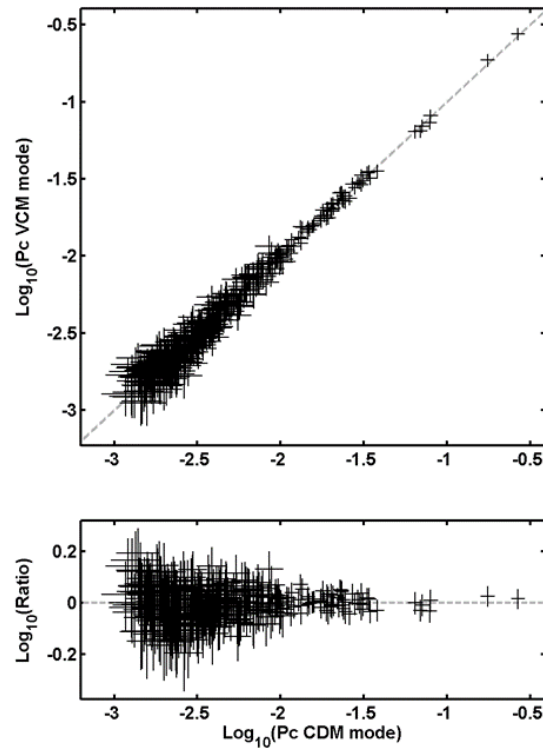


Figure 2. Comparison of BFMC CDM and VCM mode P_c estimates for 373 conjunctions.

In summary, no compellingly large deviations have been seen in P_c estimates in all of the comparison testing performed so far for temporally isolated conjunctions, which comprise the vast majority processed by the CARA system. This close alignment occurs for many of the test cases which resist non-Gaussian behavior due to implicit curvilinear construction.^{7,20,22} On the other hand, from-TCA MC approaches that sample Cartesian states¹⁹ instead of equinoctial element states can occasionally produce erroneous P_c values that differ appreciably from BFMC VCM mode estimates.

Comparisons of CDM Mode P_c Estimates and 2D P_c Approximations

Figure 3 compares P_c Y g h] a U h Y g ` WU` Wi` U h Y X` i g] approximations, for 28,652 CARA conjunctions that occurred between 2017-05-01 and 2018-03-18. These conjunctions were selected using a single criterion, $2D\text{-}P_c > 10^{-7}$, and represent events that span a large range of propagation times. The top panel shows a logarithmic plot of $2D\text{-}P_c$ (horizontal axis) vs CDM mode P_c estimates (vertical axis). The bottom panel shows the logarithm of the P_c ratio. Conjunctions shown in black do not violate the null hypothesis test³⁶ that the two P_c estimates are equal at the p-value $\leq 10^{-3}$ significance level. However, those highlighted in yellow do violate the

hypothesis at this significance level, and those in red at the higher level of p-value $\geq 10^{-6}$. Overall, Figure 3 contains 99 yellow and 52 red points, which are both much greater than the numbers expected from purely statistical variations, even though they represent a very small fraction of the original 28,652 conjunctions analyzed in this study. Major deviations occur in both directions, $CDM-P_c \ll 2D-P_c$ and $CDM-P_c \gg 2D-P_c$, with the latter type causing more concern because, for these conjunctions, the widely-employed 2D P_c approximation significantly underestimates the actual risk as indicated by the BFMC simulation. (Note, two of the conjunctions in Figure 3 with $CDM-P_c \ll 2D-P_c$ corresponded to zero hits registered in the BFMC simulations; these are represented using downward pointing triangles with a single-sided error bar directed upward.)

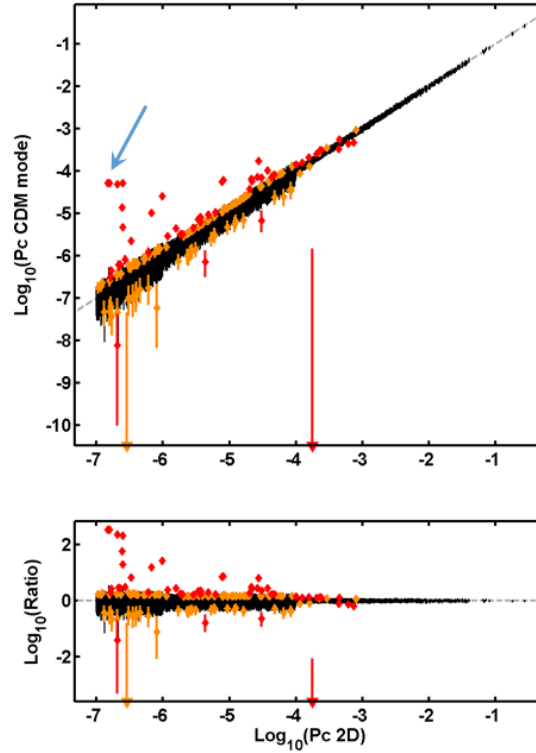


Figure 3. Comparison of BFMC CDM mode and 2D P_c estimates for 28,652 conjunctions. The blue arrow highlights the Van Allen satellite conjunction shown in Figures 4 and 5.

Many of the conjunctions with $CDM-P_c \gg 2D-P_c$ in Figure 3 have one or more of the following three characteristics: 1) involve object(s) with highly eccentric orbits, 2) have long epoch-to-TCA propagation time(s) of 10 days or more, and 3) have a relatively long interval between the nominal TCA and the time of peak probability rate. Many also correspond to two specific CARA supported missions, the Van Allen A and B satellites, both of which have highly eccentric orbits. The blue arrow in Figure 3 highlights a Van Allen conjunction possessing all three of these characteristics, including extended propagation times of (. . .) for the primary Van Allen satellite, and (. . .) for the secondary debris object, as well as a relatively long delay of about 4.5 seconds between TCA and peak probability rate. Figure 4 plots the cumulative P_c and P_c rate for this conjunction estimated using both VCM and CDM modes, with sampling trials. The BFMC estimates are statistically equivalent, $VCM-P_c \approx CDM-P_c \approx 5 \times 10^{-5}$, but both exceed the $2D-P_c \approx 1.6 \times 10^{-7}$ approximation by a factor of about 300.

REFERENCES

1. analysis team continues to investigate the specific causes and circumstances of the infrequent but large BFMC- P_c vs 2D- P_c differences like those shown in Figures 3 and 4. Again, many coincide with conjunctions involving highly eccentric orbits, extended propagation times, or the Associated Determination of Screening (ADS) process. *International TCA Risk Assessment Workshop*, 19-20 May 2015.
2. B.D. Tapley, B.E. Schutz, and G.H. Born, *Statistical Orbit Determination*, Elsevier Academic Press, Burlington, MA, 2004.
3. > " @ " : c g h y f " U b X " < " G " : 9 g h Y D e b r i s C o l l i d e n P r o b a b i l i t y a n d] W " 5 b U " r A U b Y i] Y f " U h Y " Z c f " G d " 1 5 8 9 8 , A u g . 1 9 9 2] W Y g z i " B 5 G 5 # > G 7
4. K. Chan, *Spacecraft Collision Probability*, El Segundo, CA, The Aerospace Corporation, 2008.
5. G " " 5 " x 7 " U b c z " i G U h Y "] h Y " 7 o A A S ' S p a c e F l i g h t M e c h a n i c s M e e t i n g , " 7 U f " c " 5 P i t t s b u r g h , P A , P a p e r 0 9 - 2 3 3 , F e b . 2 0 0 9 .
6. D.A. Vallado, *Fundamentals of Astrodynamics and Applications*, 2nd ed., Microcosm Press, El Segundo, CA, 2001.
7. " " G U V c " z " 7 " " 6] b n z " 5 " G Y [Y f a U b z " i f " o f C o l l i d e n z " U b X " D " k] h \ " G d Y W] U " 4 . 5 " D Y f h i f V U h " c b A / A A S ' S p a c e F l i g h t M e c h a n i c s S p e c i a l i s t C o n f e r e n c e , G i r d w o o d , A K , P a p e r 1 1 - 4 3 5 , A u g . 2 0 1 1 .
8. 6 " F " " c k a U b " Y h " " U " " z " i 5 " B Y k " 9 a d] f] W U " " H \ Y f a c g d \ " a n d G e c " a U [b Y h] W I A A / A A S ' S p a c e F l i g h t M e c h a n i c s S p e c i a l i s t C o n f e r e n c e , H o n o l u l u , H I , P a p e r A I A A 2 0 0 8 - 6 3 4 8 , 2 0 0 8 .
9. G " > " 7 U g U "] U b X " K " B " U f _ Y f z " i 8 m b U a] W " 7 U "] V f U h] G U h Y "] h Y " 8 f U " A I A A / A A S ' S p a c e F l i g h t M e c h a n i c s S p e c i a l i s t C o n f e r e n c e , M o n t e r e y , C A , P a p e r A I A A 2 0 0 2 - 4 8 8 8 , 2 0 0 2 .
10. 5] f " : c f W Y " G d U W Y " 7 c a a U b X z " i 5 g h p h / w w w . x f i n p o l . u i l] W 8 . G h U b X U f X
11. Figure 4. Estimated cumulative P_c (top panels) and P_c rate (bottom panels) for a conjunction between one of VCM mode (left panels) and CDM mode (right panels) from a conjunction between one of BA5' G5' D' g5' JYU' cellules and a debris object. 5 " Z f] Y b X z " i H \ Y " J o u r n a l V U V] "] h m
12. of Guidance, Control, and Dynamics, Vol. 23, No. 5, pp. 769-772, 2000.
13. Comparisons of BFMC and 2D P_c Close Approach Distributions
14. Some insight into the infrequent conjunctions observed in BFMC- P_c vs 2D- P_c differences can be gained by examining the distribution of close approach distances in the b-plane of the simulations. Figures 5 illustrate the CA distributions for the same SCV as in Figure 3, shown in Figure 4, produced by MC simulations using Y b [z " U b a m p l e A . " E a c h d o t i n F i g u r e 5 r e p r e s e n t s a C A w i t h i n t h e b - p l a n e d u r i n g b u n d l e d s a m p l i n g m o d e . S p e c i f i c a l l y 9 7 0 E 8 5 k 2 0 1 4 , t h e
15. 6 Y " 5 U " h] > j c Y b " Y 7 g 5 " U b c X g] 5 h] " c 8 c d V g h U b X z " i d c & i h W Y X]] g b d U f d W p g] W b
16. CA distribution, as plotted in more detail in Appendix A, pp. 1360-1375, 2006. b-plane is very similar
17. to h " \ Y z] U b z i i g Y x i h U h d c b T i z e D e p e n d e n t U n d e r l y i n g D i s t r i b u t i o n W h U] f " m j h g r d b - p l a n e w o r d A n d S p a c e F l i g h t M e c h a n i c s M e e t i n g , W i l l i a m s b u r g , V A , P a p e r 1 5 - 2 3 3 , J a n . 2 0 1 5 .
18. ? " " 7 \ U b z " i < c j Y f] b [A A S / A I A A ' S p a c e F l i g h t M e c h a n i c s M e e t i n g , W i l l i a m s b u r g , V A , P a p e r 1 5 - 2 3 4 , J a n . 2 0 1 5 .
19. So a dot for an MC trial with zero CA miss distance, z " U b X " @ " 7 " > c " b d c b z " i H] a Y
20. > " @ " : c g h y f " U b X " < " G " : 9 g h Y D e b r i s C o l l i d e n P r o b a b i l i t y a n d] W " 5 b U " r A U b Y i] Y f " U h Y " Z c f " G d " 1 5 8 9 8 , A u g . 1 9 9 2] W Y g z i " B 5 G 5 # > G 7
21. > " @ " : c g h y f " U b X " < " G " : 9 g h Y D e b r i s C o l l i d e n P r o b a b i l i t y a n d] W " 5 b U " r A U b Y i] Y f " U h Y " Z c f " G d " 1 5 8 9 8 , A u g . 1 9 9 2] W Y g z i " B 5 G 5 # > G 7

- 22 7 " ' G U V c ` ž ' H " ' G i _ i h ž ' ? " ' <] ` ` ž ' ? " ' 5 ` Z f] Y b X ž ' 6 " ' K f
7 c j U f] U b W Y ' ; Y b Y f U h] c b ' U b X ' D f c d U [U h] c b ' 5 b U ` m g] g
AAS/AIAA Space Flight Mechanics Meeting, San Diego, CA, Paper 10-134, 2010.
- 23 F " 5 " ' 6 f c i W _ Y ' U b X ' D " ' > " ' 7 Y Z c ` Celestial Mechanics, Vol. 9 e i] b c Wh
5, pp. 303-310, 1972.
- 24 8 " ' J U ` ` U X c ž ' Í 7 c j U f] U b W Y ' H f U a] g W c f a d U h A S A I A A c z b c f ž Í G U h Y
Astrodynamics Specialist Conference, Big Sky, MT, Paper 03-526, 2003.
- 25 8 " ' J U ` ` U X c ` Updated Analytical Paths for Covariance Transformations and Op-
timizationž AAS/AIAA Space Flight Mechanics Meeting, Williamsburg, VA, Paper 15-537, 2015.
- 26 8 " H " ' < U ` ` ž ' A " 8 " ' < Y ^ X i _ ž ' U b Positive Definite State Covari-
U b W Y g ' Z c f ' 7 c ` `] g] c AAS Astrodynamics Specialist Conference, Columbia
Valley, WA, Paper 17-567, 2017.
- 27 W.H. Press, S.A. Teukolsky, W.T. Vetterling, and B.B. Flannery, *Numerical Recipes in
FORTRAN: The Art of Scientific Computing*, 2nd Ed., Cambridge University Press, New York,
NY, 1992.
- 28 B.Schilling, et al. Í C d Y f U h] c b U ` ` 9 I d Y f] Y b W Y ' k] h \ ` h \ Y ' K U ` X ' G
7 c b ^ i b Wh] c b ' 5 g g Y g g a Y b h ' Z f c a ' h AAS Astrodynamics Spe-
cialist Conference, Long Beach, CA, Paper 16-5424, 2016.
- 29 7 " ' 7 ` c d d Y f ' U b X Use of Confidence or Fiducial Limits Illustrated in the Case of
h \ Y ' 6] Biometrika, Vol. 26, pp 404-413, 1934.
- 30 N.L. Johnson, S. Kotz, and A.W. Kemp, *Univariate Discrete Distributions*, Wiley-Interscience,
Hoboken, NJ, 1993.
- 31 L.D. Brown, T.T. Cai, A. DU g [i d h U ž ' Í = b h Y f j U ` ` 9 g h] a Statistical
Science, Vol. 16, No. 2, pp. 101-133, 2001.
- 32 J " H " ' 7 c d d c ` U ž ' Í 9 j U ` i U h] b [` h \ Y ' G \ c f h ' 9 b W c i b h Y f ' 5
a i ` AAS/AIAA Spaceflight Mechanics Meeting, Charleston SC, Paper 12-248, Feb. 2012.
- 33 6 " A " ' 6 f U i b ž ' Í H \ Y ' 9 j c ` i h] c b ' c Z ' G Y W c b X U f m ' C V ^ Y Wh
g U [AAS Astrodynamics Specialist Conference, Columbia Valley, WA, Paper 17-650, 2017.
- 34 J " H " ' 7 c d d c ` U ž ' > " ' K c c X V i f b ž ' U b X ' F " ' < i ^ g U _ ž ' Í 9 Z Z Y
W f U Z h ' 7 c ` `] g AAS/AIAA Spaceflight Mechanics Meeting, Wailea Maui, HI, Paper
04-181, Feb. 2004.
- 35 S. Casali, D. Hall, D. Snow, M. Hejduk, L. Johnson, B. Skrehart, and L. Baars, Í 9 Z Z Y Wh-
7 c f f Y ` U h] c b ' c Z ' C f V] h U ` ` 9 f f c f ' AAS Astrodynamics Spe-
cialist Conference, Snowbird, UT, Paper 18-272, Aug. 2018.
- 36 1, 6 7 6 (0 \$ 7 (2 b [3] b Y Y f] b [` G h E-Handbook of Statistical Methods, Sec-
tion 7.3.3, <https://www.itl.nist.gov/div898/handbook/prc/section3/prc33.htm>, 2018. Also see
<https://www.itl.nist.gov/div898/software/dataplot/refman1/auxillar/binotest.htm>, 2018.
- 37 A. Sergeyevsky, G. Snyder, R. Cuniff, *Interplanetary Mission Design Handbook, Volume 1, Part
2. Earth to Mars Ballistic Mission Opportunities, 1990-2005*, NASA JPL Publication 82-43, 1983.

